Correlated Superconducting and Insulating States in Twisted Trilayer Graphene Moiré of Moiré Superlattices

Kan-Ting Tsai[1†], Xi Zhang[1†], Ziyan Zhu[2], Yujie Luo[1], Stephen Carr[2], Mitchell Luskin[3], Efthimios Kaxiras[2, 4], Ke Wang[1*]

[1] School of Physics and Astronomy, University of Minnesota, Minneapolis, MN 55455, USA; [2] Department of Physics, Harvard University, Cambridge, MA 02138, USA; [3]School of Mathematics, University of Minnesota, Minneapolis, MN 55455, USA; [4] John A. Paulson School of Engineering and Applied Sciences, Harvard University, Cambridge, MA 02138, USA; † These authors contributed equally to this work; *To whom the correspondence should be addressed: kewang@umn.edu

Layers of two-dimensional materials stacked with a small twist-angle give rise to beating periodic patterns on a scale much larger than the original lattice, referred to as a "moiré superlattice". When the stacking involves more than two layers with independent twist angles between adjacent layers it generates "moiré of moiré" superlattices, with multiple length scales that control the system's behavior. Here, we demonstrate these effects of a high-order moiré superlattice in twisted trilayer graphene with the twist angles chosen to be equal, at ~ 3.06°. We report superconducting and correlated insulating states near the half filling of the moiré of moiré superlattice at a carrier density (~ 10^{10} cm^{-2}) significantly lower than any previously-reported superconductor[1]. Moreover, the temperature dependence of the measured resistances at full-occupancy (ν = -4 and ν = 4) states are semi-metallic, distinct from the insulating behavior of the twisted bilayer systems[2–4], providing a first demonstration of emergent superconductivity from single-particle states that correspond to continuous, non-isolated flat-bands. Compared to twisted bilayer graphene (tBLG)[2–8], we

find robust superconductivity with $T_c \sim 3.4$ K despite the extremely low carrier density. Our findings imply that phonons[9,10] may play a bigger role than flat bands and singular density of states[11–13] in bringing about the correlated behavior.

We report on a novel twisted trilayer graphene (tTLG) system with two independently controlled twist angles, in which three pieces of monolayer graphene are transferred on top of each other with equal twist angles of 3.06° (fig. 1a) between adjacent layers. In this platform, a "moiré of moiré superlattice" is formed by the interference of two sets of misaligned twisted bilayer superlattices (the 1-2 and 2-3 layer pairs) with the same moiré periodicity. The twist angle of 3.06° is obtained from the carrier density at half-filling by assuming the two twist angles are exactly equal, consistent with the experimental design for this device (see Supplementary Information for details). The full trilayer stack is encapsulated in hexagonal boron nitride, and bubble-free regions of a few μm in size are identified in which the interlayer relative twist is expected to be constant and homogeneous. The samples are then etched down to 3 μm × 3.5 μm size with a 1D edge contact defined at each corner (fig. 1b), allowing van der Pauw type 4-probe transport measurements. Our electronic structure calculations (fig. 1d-f) show a large enhancement of the density of states when the twist angles are equal, with no band gaps introduced by the moiré superlattice.

The closely related, but much simpler twisted bilayer graphene (tBLG) system exhibits unconventional correlated phases including Mott insulator[3] and superconducting states[2] at a "magic angle" twist near 1.08°. In this special bilayer configuration, two sets of isolated flat electronic bands emerge near the Fermi energy[14,15] which are commonly believed to lie at the heart of correlated behavior. The discovery of this intriguing correlated physics in tBLG sparked extensive theoretical[9,10,16,17] and experimental investigations[18,19] into van der Waals (vdW)

heterostructures, with emphasis on understanding the microscopic mechanism of the strong correlation and extending the model system to other twisted bilayer systems that involve graphene[20–22] or other layered materials like the transition metal dichalcogenides[23].

Recent theoretical works have proposed twisted trilayer graphene as a new platform for studying correlated states in vdW heterostructures. X. Li *et al.*[24] and S. Carr *et al.*[25] investigated trilayer graphene geometries with a single twist angle between the middle and outer layers, which has a larger magic angle compared to tBLG and can host concurrently flat-bands and Dirac states. C. Mora *et al*.[26] and B.Amorin and E.V. Castro[27] consider twisted trilayer graphene with two twist angles, showing that this system is a perfect metal.

To study the electronic properties of our tTLG device, we carried out electronic structure calculations based on a low-energy expansion around the Dirac point (see Supplementary Information for details). The system is generally incommensurate due to the presence of the third layer, which significantly increases the possible couplings between momentum states[28]. As a result, a large number of interspersed, folded bands appear near the Fermi level. When the two twist angles are equal, there is a range of values near 2° at which the bands near the Fermi level become quite flat. An example band structure of tTLG with different line cuts in momentum space is shown in figure 1d-e, exhibiting the bands with relatively low dispersion near the charge neutrality point. Another key observation is that the band structure is gapless and the low-energy, flat-band manifold is not isolated from the rest[28]. Figure 1f shows the corresponding normalized density of states (DOS). Due to the hybridization between the two bilayer moiré supercells, the tTLG system exhibits a more singular density of states and a smaller bandwidth compared to the tBLG at the same twist angle. The magnitude of the DOS near the tTLG magic angle is comparable to tBLG near its magic angle but with a slightly larger bandwidth (see Supplementary Information for a

more detailed comparison with tBLG). However, due to the connected bands in the system, tTLG does not have a sharp singularity in the density of states or perfectly flat bands as in magic angle tBLG.

Figure 2a shows the measured four-probe resistance at zero magnetic field, as a function of carrier density and temperature. At a carrier density around 3.11×10^{10} cm^{-2}, we observe that the resistance first decreases (corresponding to metallic behavior) from 20 K to 4 K, and then increases (insulating behavior) from 4 K down to 10 mK. We identify this to be the correlated insulator state corresponding to the half-filling, similar to that in tBLG[2,4]. Two superconducting domes are also found on either side of the half-filling insulating state below the same critical temperature $T_c \sim 4$ K, which implies that correlated phases emerge below this critical temperature in our device. The span of the superconducting domes, as well as the carrier density at which each state was found, is about two orders of magnitude smaller than those in all the previously reported twisted bilayer systems. The low carrier density suggests that the observed correlated states are near the half-filling of the tTLG moiré of moiré supercell (instead of the simple moiré supercells from either the 1-2-layer pair or the 2-3-layer pair in our tTLG device), which we estimate to be two orders of magnitude larger in area compared to the previously-reported tBLG moiré supercell. The carrier density for superconductivity is lower than any previously reported superconductor in general, not limited to the moiré systems.

Figure 2b shows resistance as a function of temperature, demonstrating a smooth metal-superconductor transition. Figure 2c provides further evidence of superconductivity by showing 4-probe differential resistance as a function of carrier density and applied DC bias at $T = 3$ K. Zero differential resistance states exist in two domes symmetrically against the zero bias, which is a signature of the superconducting behavior. The critical current J_c of the superconducting state at

the higher doping is also visibly smaller, consistent with the observation in fig. 2a. The *I-V* characteristics (discussed also later in connection to fig. 4c) imply a critical current J_c at 200 nA even at 3 K, several times higher than the value previously reported for tBLG, $J_c \sim 50$ nA at 0.07 K [2] Moreover, as the temperature increases above T_c, the *I-V* characteristics (fig. 2d) evolve from cubic-like dependence (superconducting state) to linear dependence (normal state), as expected from the BKT model of 2D superconductivity[29]. The power-law of each *I-V* curve taken at different temperatures indicates a BKT transition temperature of $T_{BKT} \sim 3.4$ K (fig. 2d inset), several times larger than the previously reported value $T_{BKT} \sim 1.0$ K for tBLG systems[2,4] .

The simple addition of the third graphene layer, from tBLG to tTLG, seems to significantly enhance the superconductivity, despite lowering the superconducting carrier density by nearly two orders of magnitude. This suggests that electron-phonon coupling could be responsible for the correlated behavior, as higher-frequency phonon modes[9,30] are expected from the longer wavelength moiré of moiré superlattices in our tTLG device. Another possible aspect, benefit from the extremely low carrier density[31–34], is formation of Bose-Einstein condensate. Finally, in tTLG, atomic relaxation due to strain introduced by the relative twist, localizes electrons at the AAA spots[28], which may enhance the electron localization due to an enlarged periodicity. Stronger localization implies a larger U and a smaller t/U ratio in a Hubbard-model picture, where t is roughly the flat band width and U is the Coulomb repulsion strength. Therefore, the bandwidth in tTLG does not have to nearly vanish for electron correlation to be important. However, in order to pin down the exact mechanism responsible for the observed correlation in tTLG, future experimental investigations beyond the transport measurements reported here are required. For example, a scanning transmission microscopy study could be used to determine the magnitude of U to evaluate the contribution from electron correlation[35].

Figure 3a shows the measured resistance R (in Ω) as a function of temperature spanning the entire range of band occupancy on the electron and hole sides. Resistance peaks are observed at all even fillings, as expected. To clearly demonstrate the temperature dependence of each filling, the measured conductance is plotted as a function of carrier density at different temperatures (fig. 3b) and as a function of temperature at each signature filling factor (fig. 3c). The filling factor is defined as $\nu = n/(n_s/4)$, in which n is the carrier density controlled by silicon backgate, and $n_s = 6.22 \times 10^{10}$ cm^{-2} is the carrier density corresponding to four charge carrier per moiré of moiré unit cell (full-occupancy). At ν = -4 and ν = 4, the measured resistance is similar to that of the charge neutrality point ($\nu = 0$) and displays a very weak metallic temperature dependence (more conducting at lower temperature), distinct from previously reported highly insulating gap states at ν = -4 and 4 in tBLG[2–4,36] and tDBLG[20,21]. This observation is consistent with our electronic structure result that the twisted trilayer graphene is gapless and provides the first experimental evidence that superconductivity can arise from non-isolated flat electronic bands.

In contrast to the semi-metallic behavior of the states at full occupancy, the states at half-filling exhibit a strong insulator-like temperature dependence (fig. 3c), with an activation gap of 0.168 meV at ν = -2 states (see Supplementary Information for details), consistent with the observed metal-insulator transition near ~ 3 K. The definition of insulator here is in the context of the temperature dependence only, the absolute value of the measured resistance at half-filling is in fact lower than that of semi-metallic full-occupancy and zero-occupancy states. The superconductivity states are particle-hole asymmetric. Two superconducting domes are observed (corresponding to fig. 2) near ν = -2, while two resistance dips instead of superconductivity are found near v=2 filling (labeled as $\nu = 2^-$ and $\nu = 2^+$) with strong metallic temperature dependence (fig. 3c). The widths of all resistance peaks including the charge neutrality points are on the order of 10^{10} cm^{-2}, suggesting

state-of-the-art device quality, necessary for resolving the moiré of moiré correlated states.

Assuming the two twist angles are exactly equal as intended by design, we surmise a twist angle of ~ 3.06° from the carrier density at half-filling, consistent with the experimental parameters for this device (see Supplementary Information for detail) as well as our expectations from theoretical considerations. The latter suggest that strong band hybridization leads to band flattening and reduction of bandwidth when the twist angles are equal or nearly equal. The slight discrepancy between the experimental magic angle and the predicted angle in our device can be attributed to several realistic scenarios. First, instead of a single magic angle, there is a range of angles near 2° at which the bands near the Fermi level flatten, similar to the magic angle value from continuum theory previously reported in twisted bilayer WSe_2 devices[23]. Moreover, in a realistic device, the two twist angles could differ slightly, which would give rise to a very different dominant moiré of moiré length. In addition, the in-plane lattice relaxation has not been accounted for in our electronic structure calculations, which is known to change the magic angle in tBLG[37,38]. Finally, as suggested earlier, the density of states in tTLG is never as singular as at the magic-angle structure in tBLG, and it may not need to behave as such, due to enhanced electron localization and Coulomb interactions. While our calculation finds the band to be narrowest near 2°, strong correlation may exist in a wider range of twist angles.

Figures 4a,b show magneto-transport data for the tTLG system. Due to the van der Paaw device geometry, the transport data is symmetrized to isolate the longitudinal resistances. The distances between each fan of even filling are as narrow as ~10^{10} cm^{-2}, comparable to the narrowest width of the Shubnikov-de Haas (SdH) oscillation in even the highest quality graphene devices[39]. As expected from the extremely small density span between our -4, 0, 4 insulator states, the magneto-transport in our tTLG device (figs. 4a, b) displays several sets of nearly overlapping Hofstadter

butterfly patterns due to several sets of Landau fan diagrams in extreme proximity with each other[40]. In addition to the experimentally-limited resolution of 10^{10} cm^{-2}, the indistinguishable Landau fans are also a signature of the tTLG systems due to their incommensurate nature even in the continuum limit, which means a small change in the twist angle generally does not correspond to a smooth change in the length scale. As a result, the systems are likely to have multiple important length scales. While we estimated the dominant twist angles to be equal at 3.06° based on the filling factor, we expect the twist angle to have slight spatial variation in a realistic device[41]. In contrast to tBLG, where a distribution of twist angles will simply result in an uncertainty in the origin of the Landau levels (broadening of the satellite fans), the slight spatial variation of the twist angles in tTLG can lead to widely separated moiré of moiré lengths[28]. As a result, the Landau fans cannot be traced back to a single origin. Despite the complicated Hofstadter butterfly pattern, a superconducting dome can be identified (dashed line in fig. 4b) in which zero-resistance states exist up to ~ 500 mT.

In conclusion, we have constructed a moiré of moiré superlattice in twisted trilayer graphene. The electronic structure of this geometry does not exhibit either a density of states with diverging behavior, or isolated flat bands, features that are connected and believed to lie at the heart of moiré superconductivity in the simpler twisted bilayer graphene geometry. Despite these major differences, correlated insulating states are found at half-filling of electronic bands in the moiré of moiré superlattice of our tTLG device, near which superconducting states have also been demonstrated at a record-low (compared to any superconducting material) carrier density of ~ 3.11 × 10^{10} cm^{-2} and with a record-high (compared to other moiré systems, especially those based on monolayer graphene) critical temperature of T_{BKT} ~ 3.4 K. This last observation raises the possibility that the moiré superconductivity in tTLG is related to BCS-like or BEC-like

mechanisms instead of electron correlation due to highly-degenerate electronic flat bands. In contrast to all previously reported twisted bilayer systems, we report that full occupancy (ν = -4 and ν = 4) corresponds to semi-metallic and gapless behavior. This demonstrates that an isolated flat-band is not required for the emergence of the superconductivity as long as strong correlation exists near half-filling. Our results on correlated behavior in tTLG represent unexpected behavior in sharp contrast to widely held beliefs about moiré superconductivity and raise interesting issues on its microscopic origin.

References

1. Fatemi, V. *et al.* Electrically tunable low-density superconductivity in a monolayer topological insulator. *Science* **362**, 926–929 (2018).
2. Cao, Y. *et al.* Unconventional superconductivity in magic-angle graphene superlattices. *Nature* **556**, 43–50 (2018).
3. Cao, Y. *et al.* Correlated insulator behaviour at half-filling in magic-angle graphene superlattices. *Nature* **556**, 80–84 (2018).
4. Lu, X. *et al.* Superconductors, orbital magnets and correlated states in magic-angle bilayer graphene. *Nature* **574**, 653–657 (2019).
5. Burg, G. W. *et al.* Correlated insulating states in twisted double bilayer graphene. Preprint at https://arxiv.org/abs/*1907.10106* (2019).
6. Sharpe, A. L. *et al.* Emergent ferromagnetism near three-quarters filling in twisted bilayer graphene. *Science* **365**, 605–608 (2019).
7. Yankowitz, M. *et al.* Tuning superconductivity in twisted bilayer graphene. *Science* **363**, 1059–1064 (2019).
8. Kim, K. *et al.* Tunable moiré bands and strong correlations in small-twist-angle bilayer graphene.

Proc. Natl Acad. Sci. USA **114**, 3364–3369 (2017).

9. Lian, B., Wang, Z. & Bernevig, B. A. Twisted bilayer graphene: A phonon-driven superconductor. *Phys. Rev. Lett.* **122**, 257002 (2019).
10. Wu, F., MacDonald, A. H. & Martin, I. Theory of phonon-mediated superconductivity in twisted bilayer graphene. *Phys. Rev. Lett.* **121**, 257001 (2018).
11. Dodaro, J. F., Kivelson, S. A., Schattner, Y., Sun, X. Q. & Wang, C. Phases of a phenomenological model of twisted bilayer graphene. *Phys. Rev. B* **98**, 075154 (2018).
12. Ochi, M., Koshino, M. & Kuroki, K. Possible correlated insulating states in magic-angle twisted bilayer graphene under strongly competing interactions. *Phys. Rev. B* **98**, 081102 (2018).
13. Carr, S., Fang, S., Po, H. C., Vishwanath, A. & Kaxiras, E. Derivation of Wannier orbitals and minimal-basis tight-binding Hamiltonians for twisted bilayer graphene: First-principles approach. *Phys. Rev. Research* **1**, 033072 (2019).
14. Tarnopolsky, G., Kruchkov, A. J. & Vishwanath, A. Origin of magic angles in twisted bilayer graphene. *Phys. Rev. Lett.* **122**, 106405 (2019).
15. Bistritzer, R. & MacDonald, A. H. Moiré bands in twisted double-layer graphene. *Proc. Natl Acad. Sci. USA* **108**, 12233–12237 (2011).
16. Po, H. C., Zou, L., Vishwanath, A. & Senthil, T. Origin of Mott insulating behavior and superconductivity in twisted bilayer graphene. *Phys. Rev. X* **8**, 031089 (2018).
17. Isobe, H., Yuan, N. F. Q. & Fu, L. Unconventional superconductivity and density waves in twisted bilayer graphene. *Phys. Rev. X* **8**, 041041 (2018).
18. Polshyn, H. *et al.* Large linear-in-temperature resistivity in twisted bilayer graphene. *Nat. Phys.* **15**, 1011–1016 (2019).
19. Cao, Y. *et al.* Strange metal in magic-angle graphene with near Planckian dissipation. Preprint

at https://arxiv.org/abs/1901.03710 (2019).

20. Liu, X. *et al.* Spin-polarized correlated insulator and superconductor in twisted double bilayer graphene. Preprint at https://arxiv.org/abs/1903.08130 (2019).

21. Cao, Y. *et al.* Electric Field Tunable Correlated States and Magnetic Phase Transitions in Twisted Bilayer-Bilayer Graphene. Preprint at https://arxiv.org/abs/1903.08596 (2019).

22. Chen, G. *et al.* Evidence of a gate-tunable Mott insulator in a trilayer graphene moiré superlattice. *Nat. Phys.* **15**, 237–241 (2019).

23. Wang, L. *et al.* Magic continuum in twisted bilayer WSe_2. Preprint at https://arxiv.org/abs/1910.12147 (2019).

24. Li, X., Wu, F. & MacDonald, A. H. Electronic structure of single-twist trilayer graphene. Preprint at https://arxiv.org/abs/1907.12338 (2019).

25. Carr, S. *et al.* Coexistence of ultraheavy and ultrarelativistic Dirac quasiparticles in sandwiched trilayer graphene. Preprint at https://arxiv.org/abs/1907.00952 (2019).

26. Mora, C., Regnault, N. & Bernevig, B. A. Flatbands and perfect metal in trilayer moiré graphene. *Phys. Rev. Lett.* **123**, 026402 (2019).

27. Amorim, B. & Castro, E. V. Electronic spectral properties of incommensurate twisted trilayer graphene. Preprint at https://arxiv.org/abs/1807.11909 (2018).

28. Zhu, Z., Cazeaux, P., Luskin, M. & Kaxiras, E. Moiré of moiré: Modeling mechanical relaxation in incommensurate Trilayer van der Waals Heterostructures. Preprint at https://arxiv.org/abs/1911.05324 (2019).

29. Kosterlitz, J. M. & Thouless, D. J. Ordering, metastability and phase transitions in two-dimensional systems. *J. Phys. C: Solid State Phys.* **6**, 1181–1203 (1973).

30. Koshino, M. & Nam, N. N. T. Continuum model for relaxed twisted bilayer graphenes and

electron-phonon interaction. Preprint at https://arxiv.org/abs/1909.10786 (2019).

31. Liu, X., Watanabe, K., Taniguchi, T., Halperin, B. I. & Kim, P. Quantum Hall drag of exciton condensate in graphene. *Nat. Phys.* **13**, 746–750 (2017).

32. Eisenstein, J. P. Exciton condensation in bilayer quantum Hall systems. *Annu. Rev. Condens. Matter Phys.* **5**, 159–181 (2014).

33. Anderson, M. H., Ensher, J. R., Matthews, M. R., Wieman, C. E. & Cornell, E. A. Observation of Bose-Einstein condensation in a dilute atomic vapor. *Science* **269**, 198 (1995).

34. Davis, K. B. *et al.* Bose-Einstein condensation in a gas of sodium atoms. *Phys. Rev. Lett.* **75**, 3969–3973 (1995).

35. Xie, Y. *et al.* Spectroscopic signatures of many-body correlations in magic-angle twisted bilayer graphene. *Nature* **572**, 101–105 (2019).

36. Serlin, M. *et al.* Intrinsic quantized anomalous Hall effect in a moiré heterostructure. Preprint at https://arxiv.org/abs/1907.00261 (2019).

37. Carr, S., Fang, S., Zhu, Z. & Kaxiras, E. Exact continuum model for low-energy electronic states of twisted bilayer graphene. *Phys. Rev. Research* **1**, 013001 (2019).

38. Fang, S., Carr, S., Zhu, Z., Massatt, D. & Kaxiras, E. Angle-dependent Ab initio low-energy Hamiltonians for a relaxed twisted bilayer graphene heterostructure. Preprint at https://arxiv.org/abs/1908.00058 (2019).

39. Dean, C. R. *et al.* Hofstadter's butterfly and the fractal quantum Hall effect in moiré superlattices. *Nature* **497**, 598–602 (2013).

40. Hunt, B. *et al.* Massive Dirac fermions and Hofstadter butterfly in a van der Waals heterostructure. *Science* **340**, 1427 (2013).

41. Uri, A. *et al.* Mapping the twist angle and unconventional Landau levels in magic angle

graphene. Preprint at https://arxiv.org/abs/1908.04595 (2019).

Acknowledgements

We thank Philip Kim, Allen Goldman, Paul Crowell and Hyobin Yoo for helpful experimental discussions, and Andrey Chubukov, Rafael Fernandes, Boris Shklovski, Dmitry Chichinadze, Laura Classen, and Daniel Massatt for helpful theoretical discussion. This work was supported in part by ARO MURI Award W911NF-14-0247and NSF DMREF Award 1922165. Z.Z and S.C. are supported by the STC Center for Integrated Quantum Materials, NSF Grant No. DMR-1231319. Nanofabrication was conducted in the Minnesota Nano Center, which is supported by the National Science Foundation through the National Nano Coordinated Infrastructure Network, Award Number NNCI -1542202.

Contributions

K-T. T., X. Z. and Y. L. performed the experiments, K-T. T. and X. Z. analyzed the data and fabricated the devices, K.W. conceived the device architecture and the experiment, Z. Z., S. C., E. K., and M. L. conceived, performed and analyzed the atomic simulation and band calculation.

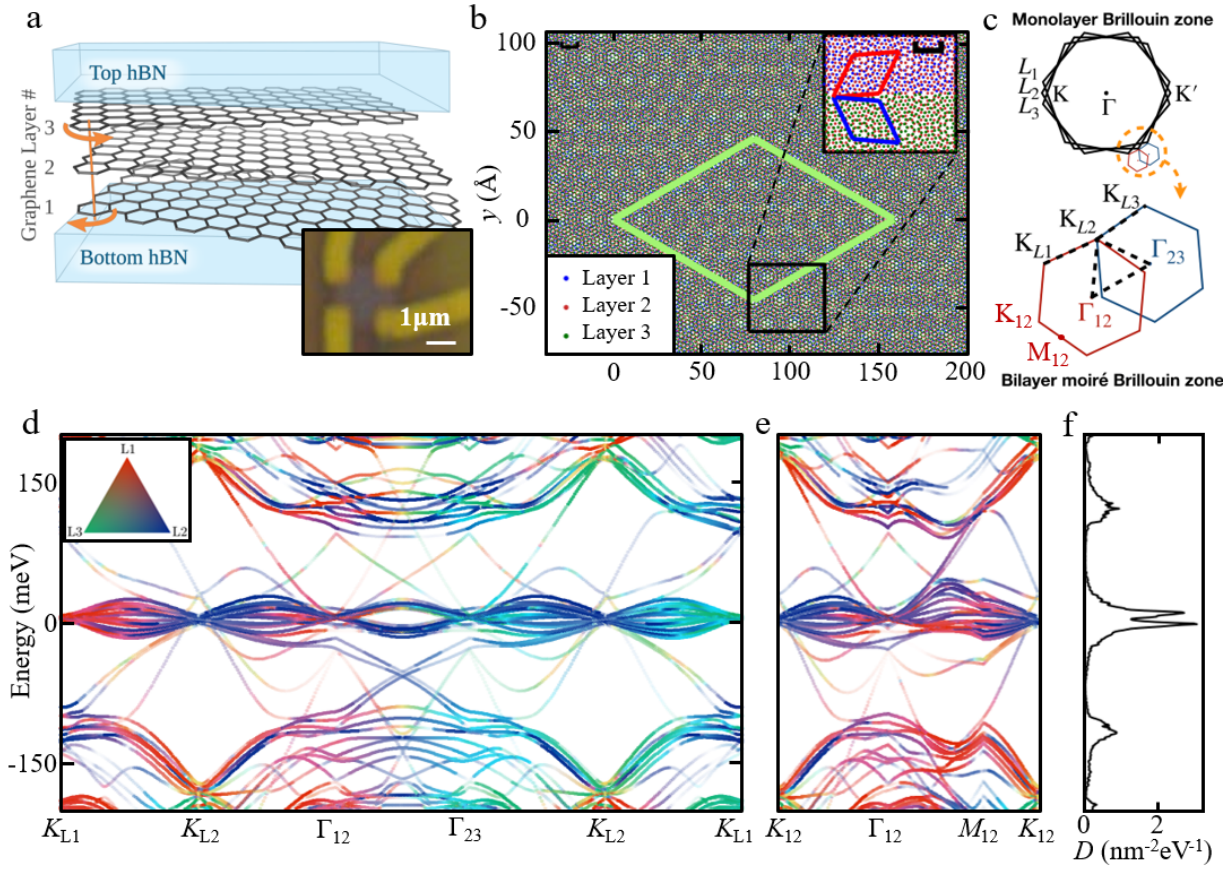

Figure 1. Moiré of Moiré Superlattices in Twisted-Trilayer-Graphene (tTLG). (a) Schematic of the hBN-encapsulated twisted trilayer graphene device. Three individual pieces of monolayer graphene are transferred on top of each other, twisted by 3.09° with respect to the previous layer (i.e., $\theta_{12} = \theta_{23} =$ 3.09°). (Inset) Optical microscope image of the device. (b) Atomic positions in twisted trilayer graphene at a set of commensurate angles $\theta_{12} = \theta_{23} = 9.43°$ demonstrating the moiré of moiré superlattice. Light green parallelogram: moiré of moiré supercell. (Inset) Zoom-in of the area inside the black box showing the bilayer moiré pattern. The top shows only layers 1 and 2; the bottom shows only layers 2 and 3; the red and blue parallelograms show the bilayer moiré supercells between layers 1 and 2 and layers 2 and 3 respectively. Both black scale bars indicate the length scale of 10 Å. (c) Monolayer Brillouin zone of the three individual layers (top) and the bilayer moiré Brillouin zone formed between adjacent bilayer pairs (bottom). High symmetry points are labelled by letters. K and K′ and related by time reversal symmetry. (d) Band structure at $\theta_{12} = \theta_{23} = 2°$ along the high symmetry line indicated by the dashed line in (c). Colors indicate the projected weight onto the state at the center momentum in each layer. Red: layer 1; blue: layer 2; green: layer 3. The color scale is shown in the triangular colormap, with the corners of the triangles showing weight purely from a single layer. (f) same as (e), along a different high symmetry line in the layers 1 and 2 bilayer moiré Brillouin zone. (f) Normalized density of states corresponding to (d) and (e).

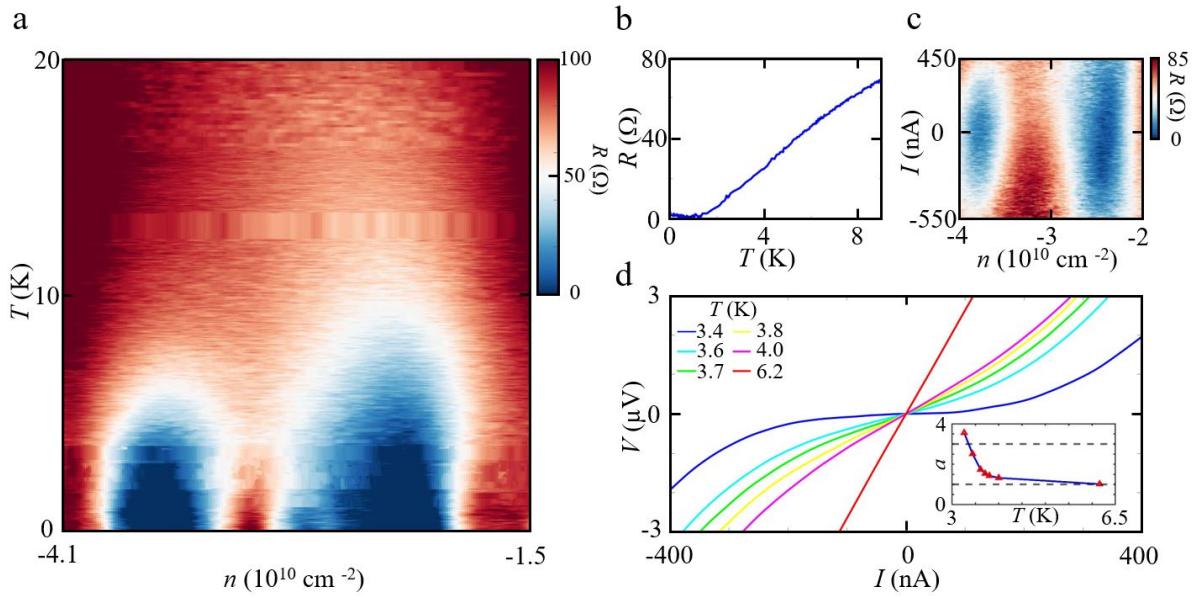

Figure 2. Temperature and Bias Characteristics of Superconductivity. (a) Measured 4-probe resistance as a function of carrier density and temperature. At half-filling of the moiré of moiré superlattice ($n \sim -3.22 \times 10^{10}$ cm^{-2}), correlated insulating behavior is observed with two adjacent superconducting domes. (b) Differential resistance as the function of temperature near the center of the right superconducting dome. (c) Differential resistance as a function of carrier density and DC bias offset at 3 K. Zero resistance states symmetric against zero bias exist up to $J_c \sim 200$ nA. (d) *I-V* characteristics at different temperatures, near the center of the right superconducting dome. The *I-V* curve power law exponent goes from 1 to 3 as temperature decreases, as expected by the BKT model of 2D superconductivity. (Inset) The temperature dependence of the power law exponent α, from which a critical temperature $T_{BKT} \sim 3.4$ K is extracted.

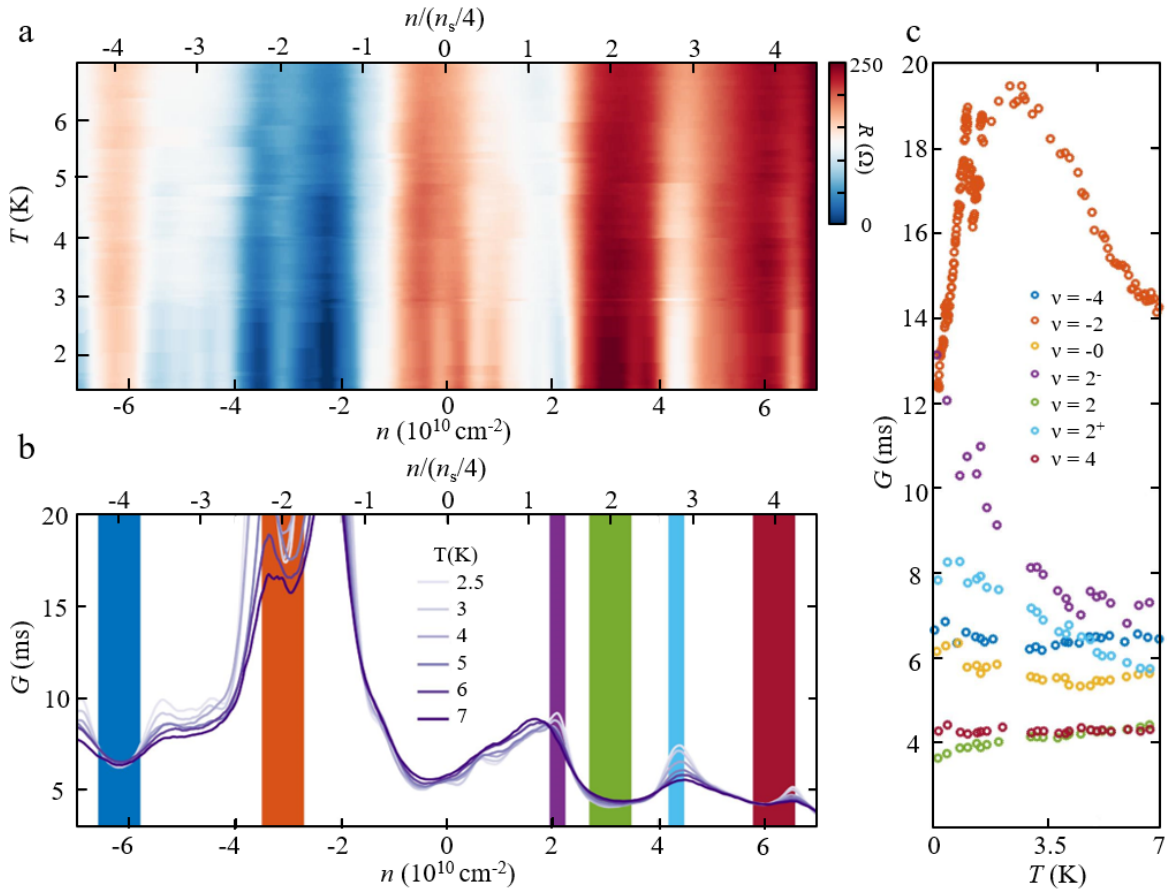

Figure 3. Insulating and Semimetal Behavior at Even Fillings of Moiré of Moiré Superlattices. (a) Measured 4-probe resistance as a function of temperature and carrier density, resistance peaks are observed at all even fillings $\nu = n/(n_s/4)$ = -4, -2, 0, 2, 4, in which n is the carrier density controlled by silicon backgate, and n_s = 6.22 x 10^{10} cm^{-2} is the carrier density corresponding to four charge carrier per moiré of moiré unit cell (full-occupancy). (b) Line traces of 4-probe conductance as a function of carrier density taken at different temperatures and (c) resistance at each even filling as a function of temperature. The full-occupancy states (ν = +/- 4) have a similar resistance and a weak temperature dependence, compared to the semi-metallic charge neutrality point (ν = 0), confirming the absence of a band gap at the full-occupancy. The ν = -2 half-filling states exhibit metallic (insulating) behavior as the measured conductance raises (lowers) at the temperature above (below) T_c ~ 3K, and two resistance dips in its vicinity evolve abruptly to superconducting states as temperature decreases. The ν = 2 half-filling states do not show strong activation behavior. Two resistance dips are also observed nearby and show strong metallic behavior as temperature lowers, but never become superconducting.

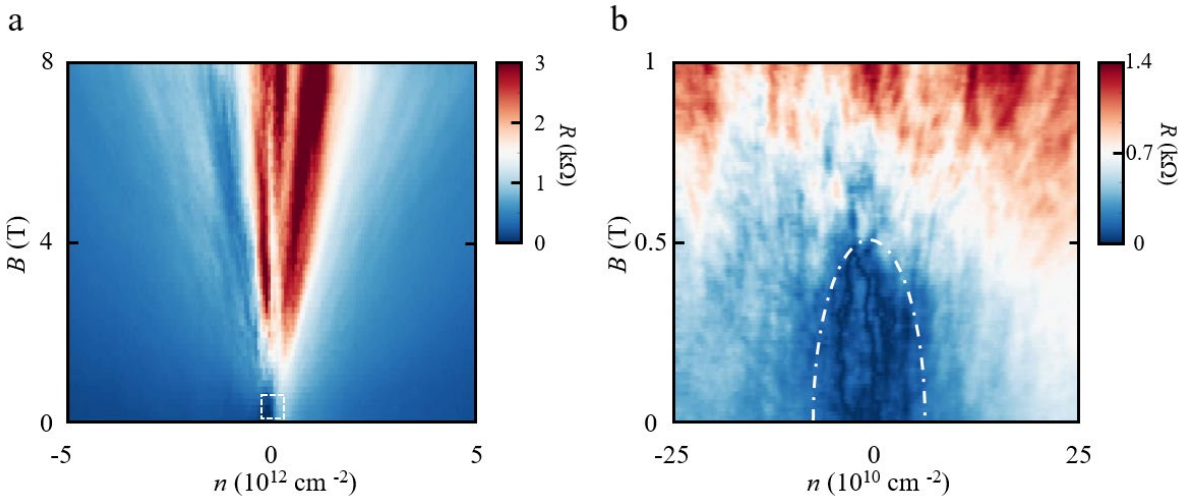

Figure 4. Magneto-Transport at Larger Carrier Density Span. (a) Resistance (*R,* in kΩ) as a function of magnetic field (*B,* in *T*) and a large range of carrier density (*n,* in 10^{12} cm^{-2}). Zero resistance states are only observed in a very small density range near zero carrier density. (b) Magneto-transport data in a smaller range of carrier density, displaying a very complicated Hofstadter butterfly pattern, in which zero resistance states exist up to ~ 500 mT.